

Purdue University
Purdue e-Pubs

International Refrigeration and Air Conditioning
Conference

School of Mechanical Engineering

2021

Hydraulic Characterization of a Adjustable Spiral-shaped Evaporator

Matthias Feiner

Universtiy of Applied Sciences Karlsruhe, Germany, matthias.feiner@hs-karlsruhe.de

Francisco Javier Fernandez Garcia

University of Oviedo

Michael Arnemann

Universtiy of Applied Sciences Karlsruhe, Germany

Martin Kipfmuller

Universtiy of Applied Sciences Karlsruhe, Germany

Follow this and additional works at: <https://docs.lib.purdue.edu/iracc>

Feiner, Matthias; Fernandez Garcia, Francisco Javier; Arnemann, Michael; and Kipfmuller, Martin, "Hydraulic Characterization of a Adjustable Spiral-shaped Evaporator" (2021). *International Refrigeration and Air Conditioning Conference*. Paper 2199.
<https://docs.lib.purdue.edu/iracc/2199>

This document has been made available through Purdue e-Pubs, a service of the Purdue University Libraries. Please contact epubs@purdue.edu for additional information. Complete proceedings may be acquired in print and on CD-ROM directly from the Ray W. Herrick Laboratories at <https://engineering.purdue.edu/Herrick/Events/orderlit.html>

Hydraulic Characterization of an Adjustable Spiral-Shaped Evaporator

Matthias FEINER^{1*}, Francisco Javier FERNÁNDEZ GARCÍA³, Michael ARNEMANN², Martin KIPFMÜLLER¹

¹Karlsruhe UAS, Institute of Materials and Processes (IMP),
76133 Karlsruhe, Germany

matthias.feiner@hs-karlsruhe.de, phone: +49(721) 925-2076

martin.kipfmüller@hs-karlsruhe.de, phone: +49(721) 925-1905

²Karlsruhe UAS, Institute of Refrigeration, Air Conditioning and Environmental Engineering (IKKU)
76133 Karlsruhe, Germany

michael.arnemann@hs-karlsruhe.de, phone: +49(721) 925-1842

³Polytechnic School of Engineering, University of Oviedo, C/Wifredo Ricart s/n,
33204 Gijón, Spain

javierfernandez@uniovi.es, phone: +34(985) 18 2112

* Corresponding Author

ABSTRACT

To ensure reliability in miniaturized devices or processes with increased heat fluxes, decreasing available cooling surfaces have to be met by novel cooling methods. In order to meet this challenge, a new type of evaporator, the swirl evaporator, was developed. The swirl evaporator is a screw-shaped cylindrical evaporator with an internal diameter between 1 – 3 mm, which is inserted as a blind hole in components with high heat generation. The refrigerant is fed into the blind hole via a capillary, deflected by 180° in the drilling base and flows out of the evaporator again in a helical way (twist flow) against the inflow direction. The refrigerant is pressed against the hot wall by centrifugal forces. This results in an increased critical heat flux. The evaporator's design allows a compact size, making it suitable for a wide range of technical applications. To enable its design for industrial needs, a test stand has been developed. The hydraulic characterization was performed by varying the evaporator length. First experimental results show a linear relationship between swirl evaporator length and pressure loss.

1. INTRODUCTION

In order to ensure operational reliability in miniaturized devices and in many technical processes with increased heat flux, decreasing cooling surfaces have to be compensated by more effective cooling methods. The new swirl evaporator type was developed to meet this challenge. The swirl evaporator is a very compact form of evaporator in which the refrigerant evaporates in a spiral (in this case the threads of a screw). The swirl evaporator is a further development of the spot evaporator which was developed and investigated by Knipping (Knipping, T., 2018). The spot evaporator is an evaporator in which the refrigerant flows through the capillary into the evaporator, is deflected at the end face of the blind hole by 180° against the inflow direction and flows partly evaporated out of the spot evaporator. Possible fields of application are the cooling of tools for plastic injection molding, the cooling of linear motors (Knipping, T. *et al.*, 2014) and the cooling of machining processes of nickel-based alloys such as Inconel 718 (Knipping, T. *et al.*, 2015). The advantages of this system are its simple manufacturability, its high heat flux and precise heat dissipation. The disadvantages are the poor controllability and energetic optimization potentials, because in the operating state usually only 20 % of the refrigerant evaporates before reaching critical heat flux (Knipping, T., 2018). In this context the spot evaporator was improved by inserting a swirl-shaped back flow of the refrigerant. The swirling geometry causes centrifugal acceleration, which causes the refrigerant to rotate around the longitudinal axis.

A profile of a swirl evaporator with a swirl-creating geometry is shown in Figure 1. Continuous improvement of products and processes has always been a major goal since the industrial revolution. Companies target to decrease the cycle time in order to rise the output in production lines and to save costs by optimized cooling methods. One way to cut costs is reducing the size of components and hence the entire product but at the same time performance needs to be the same or even improved. These contradictions result in an increased heat generation and heat dissipation for most production processes. This phenomenon of improved performance for tools and applications leading to increased process heat is described by Knipping (Knipping, T., 2018). In this application (process improvement and to ensure the required properties) high heat flux has to be dissipated in a very confined surface. Cooling of processors is one more application where a relatively high heat flux in a limited space occurs. The limitation of overclocking is mostly a limitation of cooling capacity. The limits of the ever smaller and more powerful diodes in the semiconductor industry are mostly of thermal origin. More efficient cooling with evaporating refrigerant would be one way to gain additional performance from processors. To meet these challenges, the Institute for Materials and Processes (IMP), in cooperation with the Departamento de Energía, is researching a new evaporator design. In this paper, a hydraulic characterization of the swirl evaporator is performed. A correlation-based model is presented to calculate pressure losses. Its knowledge is essential to determine the mass flow and heat transfer coefficients. For this purpose, the swirl evaporator is classified into different hydraulically active groups. Different correlations are used to describe the individual regimes. The results generated with the simulation program are compared with the data measured on the test bench in order to be able to make a statement regarding the validity of the simulation program created. Design recommendations for further performance-related improvements to the swirl evaporator derived from the simulation results are given at the end of the report. The aim is to be capable of carrying out the entire design and sizing of the swirl evaporator with this program, in order to eventually achieve a saleable product that can be adapted accurately to the processes to be performed in each case.

2. DESCRIPTION OF THE TEST CARRIER

As shown in Fig. 1, the hydraulically active parts of a swirl evaporator are a cylindrical pocket hole with an internal diameter of 4.5 mm in which a screw turned to fit is inserted. A through-hole of 0.85 mm in diameter was eroded into the screw. A capillary made of rolled stainless steel with an outer diameter of 0.8 mm and an inner diameter of 0.5 mm is guided in this through-hole. On the right side of the capillary a fitting is soldered to connect the swirl evaporator to the rest of the refrigeration system.

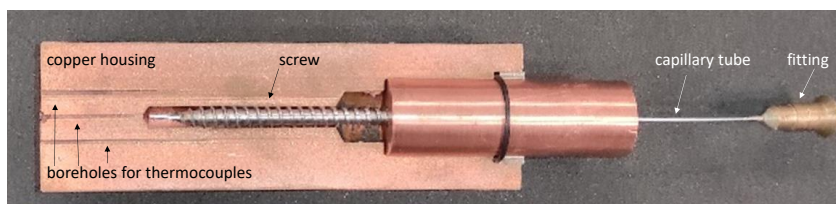


Figure 1: Profile of a swirl evaporator with hydraulically relevant parts

The extended swirl evaporator model basically consists of 4 hydraulically relevant groups: the sudden cross-section reduction from the feed line to the capillary tube in the fitting; the capillary tube, the spray and the swirl flow in the screw. Fig. 2 shows the 4 hydraulically relevant groups and 6 regimes considered. The capillary tube consists of the regimes of single-phase (subcooled liquid) and, if necessary, two-phase, and the subgroup of swirl flow into a two-phase and, if necessary, superheated (single-phase). The 4 groups of the swirl evaporator can thus be divided into 6 regimes, see Fig. 2. Within a regime, a part of the swirl evaporator can be unified, for which the thermohydraulic change of state of the flow can be quantified with the same empirical calculation model. The regimes are composed of a sudden cross-sectional constriction (widely protruding angular inlet or Borda orifice), the capillary tube with a one- and two-phase region, the spray and swirl region again with a two-phase region, and any superheat that may occur.

The refrigerant mass flow \dot{m} enters the swirl evaporator through the capillary tube, which causes a pressure drop due to frictional losses. Depending on the pressure drop in the capillary tube (mainly a function of hydraulic diameter, length and flow velocity), a two-phase condition may occur. After injection, the refrigerant is directed into the swirl at the hot face of the blind hole, where it evaporates and possibly overheats. In the test carrier of the swirl evaporator,

an electric heating jacket transfers the heat load into the system via the outer surface of the cylinder. The relatively high thermal conductivity of the test vehicle's copper housing distributes the heat. The heat is dissipated in the blind hole by the evaporating refrigerant.

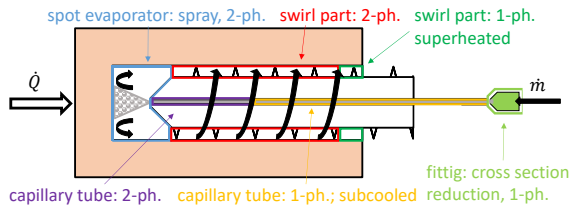


Figure 2: Regimes of a swirl evaporator

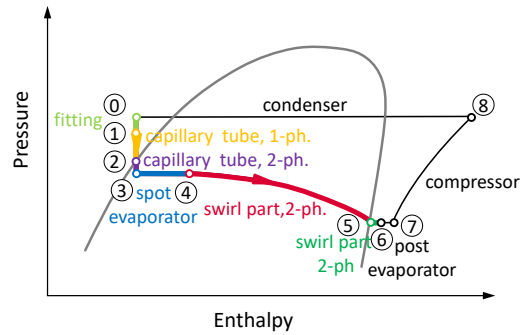


Figure 3: Cycle process in the swirl evaporator in the pressure-enthalpy diagram

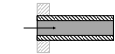
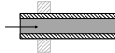
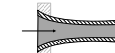
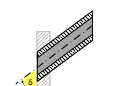
The cycle process of the refrigerant is shown in Fig. 3. The bold red line shows the process steps that take place in the swirl evaporator itself, while the thin black line shows those process steps that are outside the swirl evaporator and do not differ from an ordinary refrigeration cycle. The refrigerant flows through the fitting, which is a sudden cross-section narrowing from 6 mm to 0.5 mm, into the capillary tube (0→1). Depending on the mass flux the capillary tube can be divided into a single phase (1→2) and if the situation arises a two-phase pressure drop (2→3), due to the frictional pressure losses. At the capillary outlet, it expands as a spray channel onto the end face of the pocket hole (3→4). In this area of spray cooling, also called spot evaporator, the refrigerant evaporates almost isobarically. The counterflow enters the screw threads against the inflow direction and continues to evaporate (4→5). This area is also called the swirl part of the evaporator. If the heat input is above the latent heat, the refrigerant will already overheat in this area (5→6). For compressor safety there is also an additional post evaporator in the test bench to assure a fixed overheating of the refrigerant (6→7) before it enters the compressor and is compressed to condensation pressure (7→8) and condensates in the condenser and gets subcooled in an additional heat exchanger (8→0). A full description of the test facility where the experiments took place, the system operating conditions and uncertainties can be found in (Feiner *et al.*,2018).

3. HYDRAULIC CHARACTERIZATION AND SETUP OF THE MODEL

In order to setup a simulation model, appropriate correlations which describe the 4 hydraulically active areas and its 6 different regimes need to be found. At the inlet of the swirl evaporator, there is a sudden narrowing of the cross-section. Since the capillary tube projects far into the wider tube area of the condenser outlet, the assumption is made here of a Borda orifice is assumed. This is defined in (Bohl, W. & Elmendorf, W., 2005) as

$$\Delta p = \zeta_E \cdot \frac{\rho}{2} \cdot w^2. \tag{1}$$

Table 1: Inlet dependent pressure loss coefficients (Bohl, W. & Elmendorf, W., 2005)

Edged inlet	very sharp	$\zeta_E = 1.69$	
	normally broken	$\zeta_E = 0.5$	
Wide protruding edged inlet	very sharp	$\zeta_E = 3$	
	(Borda orifice)		
Rounded inlet	depending on smoothness from	$\zeta_E = 0.005$	
	to	$\zeta_E = 0.05$	
	usually	$\zeta_E = 0.06$	
Angular inlet under angle δ (normally broken)		$\zeta_E = 0.5 + 0.3 \cos \delta + 0.2 \cos^2 \delta$	

In addition, it is assumed that the change of state takes place without an enthalpy change. In areas in which the refrigerant flows in a two-phase state, the liquid and gaseous phases are described collectively in one model. This means that the model describes them with the same flow velocity. However, the two phases have different fluid properties. The kinematic viscosity of the two-phase flow is modeled according to the mixing model described in (Akers *et al.*, 1959)

$$v_{tp} = \frac{v_L}{1 - x + x \cdot \left(\frac{\rho_L}{\rho_G}\right)^{0.5}} \quad (2)$$

For the calculation of the pressure drop within a regime, the Reynolds number is calculated according to the correlations taken from the VDI Heat Atlas (Wellenhofer, A., p.1293, 2019). For Reynolds numbers smaller than 2320, i.e. laminar flows, the Hagen-Poiseuille law (Poiseuille, J. M. L, 1846)

$$\zeta = \frac{64}{Re} \quad (3)$$

applies to determine the drag coefficients. For turbulent flows and in the range of Reynolds numbers between 3000 and 100,000, the following equation is used (Kind, M., 2019)

$$\zeta = \frac{0.3164}{\sqrt[4]{Re}} \quad (4)$$

and in the range of Reynolds numbers between 10^4 and 10^6 the Konakov equation (Konakov, P. K., 1946)

$$\zeta = (1.8 \cdot \log_{10}(Re) - 1.5)^{-2} \quad (5)$$

can be used. For the two-phase pressure loss in the capillary tube, a correlation for straight horizontal lines is used and only the pressure loss due to friction is considered in this approach. The acceleration part due to the low evaporation in the capillary is neglected. For unknown flow patterns, the approach of Garcia as described in (Wellenhofer, A., 2019)

$$\Delta p_{tp} = \frac{\Delta L \cdot 2 \rho_M w_M^2}{D} \left(0.0925 \cdot Re^{-0.2534} + \frac{13.98 \cdot Re^{-0.9501} - 0.0925 \cdot Re^{-0.2534}}{\left(1 + \left(\frac{Re}{293}\right)^{4.864}\right)^{0.1972}} \right) \quad (6)$$

is suitable. The mixture density is determined based on the equation

$$\rho_M = \rho_L \cdot \lambda_L + \rho_G \cdot (1 - \lambda_L). \quad (7)$$

The volume flow rate λ_L is calculated using the equation

$$\lambda_L = \frac{\dot{V}_L}{\dot{V}_L + \dot{V}_G}. \quad (8)$$

The empty pipe gas velocity w_G can be determined using

$$w_G = \frac{\dot{V}_G}{A} = \frac{\dot{m} \cdot x}{\rho_G \cdot A}. \quad (9)$$

and empty pipe liquid velocity w_L can be calculated using

$$w_L = \frac{\dot{V}_L}{A} = \frac{\dot{m} \cdot (1 - x)}{\rho_L \cdot A}. \quad (10)$$

Averaging both velocities gives the mean flow velocity w_M .

The liquid phase has the dominant share in the total pressure drop. Therefore, the average Reynolds number is calculated exclusively with the viscosity for the liquid phase according to

$$Re = \frac{w_M \cdot D}{\nu_L} . \quad (11)$$

For the regime in the spray region, a correlation presented in (Roul, M. & Dash, S., 2011) was used. The equation considers a two-phase condition when spraying from the capillary under the influence of the counterflow. As shown in Fig.4, the model assumes expansion due to a sudden change in cross-section up to half the bore diameter. In the other half of the bore diameter, the reverse flow takes place in the model. The two-phase pressure drop $\Delta p_{tp,spray}$ consists of the product

$$\Delta p_{tp,spray} = \Delta p_0 \cdot \gamma_{spray} \quad (12)$$

The factor γ_{spray} is calculated according to the equations

$$\gamma_{spray} = 1 + \left(\left(\frac{v_G}{v_L} \right) - 1 \right) \cdot (B \cdot x \cdot (1 - x) + x^2) \quad (13)$$

$$B = \left(\frac{1}{k_{slip}} \right)^{0.28} . \quad (14)$$

For $X_{xp} > 1$ holds

$$k_{slip} = \left(\frac{v_G}{v_L} \right)^{0.25} \quad (15)$$

and for $X_{xp} \leq 1$

$$k_{slip} = 1 + x \cdot \left(\frac{v_G}{v_L} - 1 \right)^{0.5} . \quad (16)$$

The size X_{xp} is calculated according to the equation

$$X_{xp} = \frac{1 - x}{x} \cdot \left(\frac{v_L}{v_G} \right)^{0.5} \quad (17)$$

The equation for determining Δp_0 applies to the single-phase pressure drop

$$\Delta p_0 = \frac{\zeta_{Spray} \cdot G^2 \cdot v_L}{2} \quad (18)$$

$$\zeta_{Spray} = \left(-\frac{2}{\sigma_{ar}} \right) \cdot \left(1 - \left(\frac{1}{\sigma_{ar}} \right) \right) \quad (19)$$

$$\sigma_{ar} = \frac{1}{4} \frac{D_{evap}^2}{d_{capillary}^2} \quad (20)$$

A correlation by Guo (Guo, L. *et al.*, 2001) is used to determine the pressure drop in the two-phase region of the swirl. It is a modified correlation by Chen (Chen, L., 1984) for straight tubes with experimental data for swirl flow. It is noticeable that the pitch of the helix is not considered. The equations were obtained using the refrigerant R718, with a helical tube diameter of 10 mm, a diameter ratio $D_{evap}/D_{hyd,swirl}$ between 13 and 25, pressures between 5 and 35 bar, and mass flows between 150 and 1760 kg m⁻²s⁻¹. Since R718 and R32 differ greatly in liquid and gaseous states, deviations must be expected. However, since the helix geometry is well suited for this application, it was chosen.

$$\Delta p_{tp,swirl} = \Phi \cdot \Delta p_0 \quad (21)$$

$$\Phi = 142.2 \cdot \psi \cdot \left(\frac{p}{p_{krit}}\right)^{0.62} \cdot \left(\frac{d}{D}\right)^{1.04} \cdot \left(1 + x \cdot \left(\frac{\rho_L}{\rho_G} - 1\right)\right) \quad (22)$$

with:

$$\psi = 1 + \frac{x \cdot (1 - x) \cdot \left(\frac{1000}{G} - 1\right) \cdot \left(\frac{\rho_L}{\rho_G}\right)}{1 + \varphi \cdot \left(\frac{\rho_L}{\rho_G} - 1\right)} \quad (23)$$

for $G < 1000 \text{ kg m}^{-2} \text{ s}^{-1}$: $\varphi = x$ and for and for $G \geq 1000 \text{ kg m}^{-2} \text{ s}^{-1}$ $\varphi = 1 - x$. Since the cross-section of the channel in the helical turns deviates from the circular shape, the hydraulic diameter d_{hyd} is used here to calculate the pressure loss. The definition of the hydraulic diameter, as shown in Fig. 5, is based on the idea that comparable conditions exist when the cross-sectional area A_{hyd} and the circumference P_{hyd} are in the same ratio. Here, when considering the cross section, the wetted perimeter is the length of the curve where the fluid contacts the pipe wall

$$d_{hyd} = 4 \cdot \frac{A_{hyd}}{P_{hyd}} \quad (24)$$

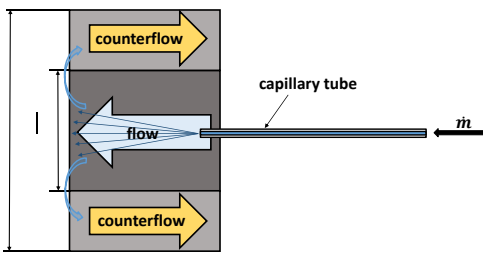


Figure 4: Illustration of spraying from the capillary tube with a sudden change in cross-section (Roul, M. & Dash, S., 2011)

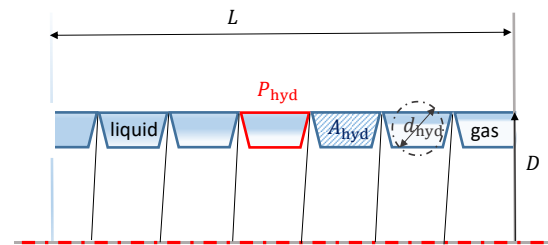


Figure 5: Hydraulic diameter of a swirl evaporator

The Nusselt correlation for calculating the heat transfer in the spray area comes from. (Lindeman, B. A. *et al*, 2013) based on the work of Goldstein (Goldstein, R. J. & Franchett, M. E., 1988) for the fluid air. This modification makes the correlation applicable to other refrigerants. By modification, Lindeman et al (Lindeman, B. A. *et al*, 2013) allowed the application to other unspecified fluids. The correlation for the Nusselt number is

$$Nu_{spray} = Re_{d_{capillary}}^{0.7} \cdot Pr^{1/3} \cdot A \cdot e^{-(B_{Nu} + C_{Nu} \cdot \cos(\phi)) \cdot \left(\frac{l_{wk}}{d_{capillary}}\right)^m} \quad (25)$$

$$A_{Nu} = -1.45 \cdot 10^{-4} \cdot \left(\frac{l_{wk}}{d_{capillary}}\right) + 0.151 \quad (26)$$

$$B_{Nu} = 0.18 \cdot \theta^2 - 0.54 \cdot \theta + 0.78 \quad (27)$$

$$C_{Nu} = 0.16 \cdot \theta^2 - 0.67 \cdot \theta + 0.66 \quad (28)$$

To determine the heat transfer in the two-phase swirl region, a correlation of Yagov (Yagov, V. V., 2005) is used. This is based on the heat flow by bubble boiling and for convective heat transfer from chapter 6.5 of (Wellenhofer, A., 2019). The material properties are determined according to the viscosity model, since a single-phase fluid state is assumed for the correlation. To cause centrifugal acceleration of the refrigerant against the hot wall, Yagov inserted a twisted band into the cylindrical sleeve.

$$q_b = 3.43 \cdot 10^{-4} \cdot \left(\frac{\lambda^2 \cdot \Delta T_s^3}{\nu \cdot \sigma \cdot T_s} \right) \cdot \left(1 + \frac{h_{LG}}{2 \cdot R_i \cdot T_s^2} \Delta T_s \right) \cdot \left(1 + \sqrt{1 + 800 B_{Nu,tp} + 400 B_{Nu,tp}} \right) \quad (29)$$

$$B_{Nu,tp} = \frac{h_{LG}}{\sigma} \cdot \left(\frac{(\nu \cdot \rho_G)^3}{\lambda \cdot T_s} \right)^{0.5} \quad (30)$$

$$\Delta T_s = T_w - T_s \quad (31)$$

The share of heat transfer by bubble boiling predominates only for heat flux $> 8 \text{ MW m}^{-2}$ and mass flow rates above $56,000 \text{ kg m}^{-2}\text{s}^{-1}$ (Yagov, V. V., 2005). In the application studied here, heat flux density is 0.1 MW m^{-2} in the swirl region and 13 kW m^{-2} in the spray region. The influence of bubble boiling on heat transfer with large differences in absolute amounts to the convective heat flux fraction is described by the equation

$$q = (q_c^3 + q_b^3)^{1/3} \quad (32)$$

At high mass flow rates, both heat transfer mechanisms act independently and may superimpose. Lopina and Bergles (Lopina, R. F. & Bergles, A. E., 1969) carried out experiments with the fluid water at pipe diameters of 5 mm and developed an empirical correlation for the single-phase heat transfer coefficient. It has the best agreement with test results for liquid fluid heating (Yagov, V. V., 2005). The simulation evaluation uses diameters of the Evaporators D_{evap} between 8 and 14 mm. From this comparison, differences between the screw and the twisted tape can be expected in addition to the geometrical deviation. The improvement in heat transfer due to the twisted flow was formalized in the correlation by 3 factors. The heat flux component is represented by

$$\alpha_s = \frac{\lambda}{D_{\text{hyd}}} F \left(0.023 (k_1 \cdot Re_{\text{hyd}})^{0.8} \cdot Pr^{0.4} + 0.193 \left(\left(\frac{Re_{\text{hyd}}}{y} \right)^2 \frac{D_{\text{hyd}}}{D_i} \beta \Delta T Pr \right)^{1/3} \right) \quad (33)$$

The first term of the equation is equivalent to a common correlation for convective heat transfer for a smooth, straight pipe, consisting of a product of Prandtl and Reynolds number adjusted with the correction factor k_1 due to increase in axial velocity

$$k_1 = \left(1 + \frac{\pi^2}{4 y^2} \right)^{0.5} \quad (34)$$

The second term of the equation takes into account the non-uniform density distribution in the swirl flow area due to the mass forces caused by the centrifugal acceleration. The surface and material properties of the fins of the twisted belt are considered by the factor F . However, it is not necessary to consider F for the application here, because the swirl evaporator is equipped with a threaded screw. Since no more suitable alternatives were found to describe the heat transfer mechanisms in the swirl region, this relationship was retained. Changes of state between capillary inlet and swirl outlet considering pressure losses and heat flow are quantified by the model. The program consists of a main program and several procedures (subroutines). With the correlations of the individual regimes implemented in the respective subroutines, the pressure loss is calculated for a given initial value for the mass flow and other operating parameters. In this process, the heat transfer and pressure drop are determined independently of each other. The mass flow is first adjusted with a defined step size of 1000 Pa in iterations until a given tolerance deviation between the target evaporating pressure and the simulated evaporating pressure is reached. With the mass flow rate determined, the heat transfer is calculated in the second step. This procedure is also used for the correlations of the heat transfer in the spray, single-phase and two-phase swirl regimes. In a preceding FEM simulation, the distribution of the heat flows was determined. About 95 % of the heat is dissipated via the almond surface (swirl) and about 5 % via the front surface (spray regime). The simulation is deterministic, i.e. starting from an initial value for the mass flow, all correlations for the pressure drop are calculated chronologically along the regimes and at the end of an iteration the deviation from the target evaporating pressure is calculated. Depending on whether the error is positive or negative, the mass flow is increased or decreased by one increment. This is repeated until the value falls below a specified tolerance deviation. The parameterization Nusselt correlation for the spray is supplemented by 2 correction factors K_1 and K_2 and has the form

$$Nu_{\text{spray}} = K_1 \cdot Re_{d,\text{capillary}}^{0.7 \cdot Pr^{1/3}} \cdot A_{Nu,\text{spray}} \cdot e^{\left(- (B_{Nu,\text{spray}} + C_{Nu,\text{spray}} \cdot \cos(\phi)) \cdot \left(\frac{l_{wk}}{d_{\text{capillary}}}\right)^m\right)} - K_2 \quad (35)$$

The correction factor K_1 is changed by one increment during an iteration, while K_2 is static. K_1 is changed until the deviation is less than 1 W. For an easier parameterization of the Nusselt-correlation for the swirl part the correction factor K_1 is adopted as a factor to the heat transfer correlation in the swirl in the equation

$$\dot{q}_{\text{swirl}} = K_1 \cdot (q_{c,\text{swirl}}^3 + q_{b,\text{swirl}}^3)^{1/3} \cdot A_{Nu,\text{swirl}} \quad (36)$$

4. EXPERIMENTAL VALIDATION

To verify the simulation results, a series of measurements were performed on the test rig described in (Feiner, M. *et al.*, 2018). Tests were carried out with different bolt grip lengths under steady-state conditions in a controlled and air-conditioned environment. Each test was repeated at least 3 times. A screw engagement length of 0 mm means that the test was performed without a screw as shown in Fig. 6c. “Without screw” also corresponds to the equivalent of the spot evaporator.



Figure 6: Various penetration depths of the screw

The measured mass flow is used to calculate the pressure drop of the simulation. The point corresponds to the arithmetic mean of the measurement series of an engagement length and the error bar corresponds to a standard deviation. Since the screw engagement lengths in the test are subject to a certain measurement uncertainty, which does not occur in the simulation, error bars are entered on the abscissa only for the test results.

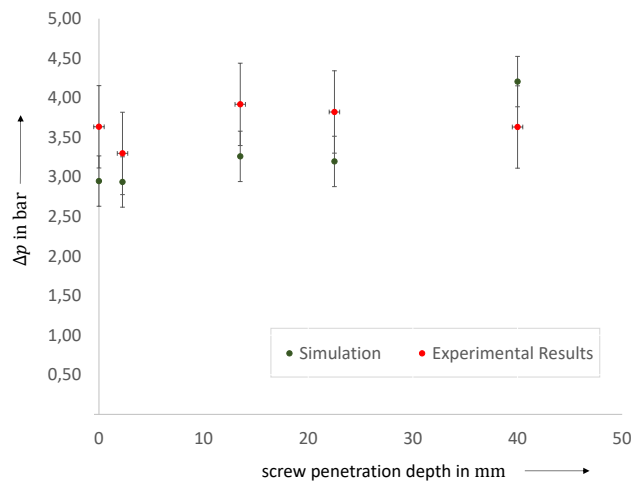


Figure 7: Comparison of the simulation to the experimental results

Overall, the results obtained in the experiment show a good correlation with the calculated values. For penetration depths smaller than 25 mm, the simulation seems to underestimate the pressure drop, and for a penetration depth of 40 mm, the simulation overestimates the measured values. This could be due to the changed flow pattern caused by the longer swirl length. Or to the phenomenon, already observed by Katto (Katto, Y.,1978; Katto, Y.,1979; Katto, Y.,1980) that under certain circumstances the total pressure drop can practically also be lower than the pressure drop that would result if the fluid would continue to flow adiabatically under the conditions at the inlet to the evaporator

tube. This is the case if the fluid still flows out subcooled, although subcooled boiling has already taken place, and is not currently considered in the model.

6. CONCLUSION

In this work, a hydraulic characterization of a swirl evaporator was carried out. Models for describing its thermodynamic behavior were presented and verified in experiments. The models can be used to design or optimize a swirl evaporator. The simulation model can calculate the pressure drop in the swirl evaporator with an acceptable accuracy of less than a standard derivative. With this step done it is now possible to hydraulically optimize the swirl evaporator regarding a minimization of the pressure loss in the swirl part.

NOMENCLATURE

A	area of the flow cross section	m^2
D_{evap}	diameter evaporator	m
D_i	inner diameter	m
F	surface and material properties factor of the twisted strip	–
G	mass flow density	$kg\ m^{-2}s^{-1}$
h_{LG}	evaporation enthalpy of the fluid	kJ/kg
l_{wk}	distance between capillary outlet and cooling wall	m
m	experimental factor	–
Pr	Prandtl-number	–
q	heat flux	$W\ m^{-2}$
Re	Reynolds-number	–
T_s	temperature of the swirl flow	K
T_w	temperature effective heat transfer surface (wall)	K
U	circumference of the flow cross section	m
w_G	pipe gas velocity	$m\ s^{-1}$
X_{xp}	mixed quality	–
x	quality	–
y	pitch at 180° rotation related to the diameter of the screw	–
α	heat transfer coefficient	$W\ m^{-2}K^{-1}$
γ_{Spray}	factor for the calculation of the pressure drop of the spray	–
Δp_0	difference of the evaporation pressure	Pa
ΔT	difference temperature	K
ζ	drag coefficient	–
η	dynamic viscosity	$kg\ m^{-1}s^{-1}$
θ	spray angle in radiant	–
k_{slip}	correlation factor for pressure loss	–
λ	thermal conductivity of a fluid	$W\ m^{-1}K^{-1}$
λ_L	volume flow portion liquid phase	–
ν	kinematic viscosity	$m^2\ s^{-1}$
ρ	density	$kg\ m^{-3}$
σ	surface tension	$N\ m^{-1}$
Φ	two-phase multiplier swirl flow	°
ψ	coefficient for two-phase pressure drop calculation	–

REFERENCES

- Akers, W. W., Deans, H. A. and Crosser, O. K. (1959). Condensation Heat Transfer within Horizontal Tubes, *Chemical Engineering Progress Symposium Series*, Vol. 55, No. 29, 171–176.
- Bohl, W., Elmendorf, W. (2005). *Technische Strömungslehre*, Vogel Fachbuch (Kamprath-Reihe)
- Chen, L. (1982). Steam-water two-phase flow frictional pressure drop in straight tubes, in: Chen 955X., *Selected papers of multiphase flow and heat transfer, Paper 7*, Xi'an Jiaotong 956 University Press, 7.1–7.6.
- Feiner, M., Arnemann, M., Fernández García, J. F., Kipfmüller, M. (2021). Hydraulic Optimization of an Adjustable Spiral-Shaped Evaporator, *Proceedings of the International Conference on Thermal Science and Engineering Applications*, Singapore, 11. –12. January 2021.
- Feiner, M., Kipfmüller, M., Arnemann, M. (2018). Development of an Adjustable Spiral-shaped Evaporator, *Proceedings of the 17th International Refrigeration and Air Conditioning Conference at Purdue*
- Gnielinski, V. (1995). Ein neues Berechnungsverfahren für die Wärmeübertragung im Übergangsbereich zwischen laminarer und turbulenter Rohrströmung, *Forsch Ing-Wes 61*, 240–248
- Gnielinski, V. (1975). Neue Gleichungen für den Wärme- und den Stoffübergang in turbulent durchströmten Röhren und Kanälen, *Forschung im Ingenieurwesen (Engineering Research)*, 41 , 8–16
- Goldstein, R. J. and Franchett, M. E. (1988). Heat transfer from a flat surface to an oblique impinging jet, *Journal of Heat Transfer*, 110(1), 84–90
- Guo, L., Feng, Z., Chen, X. (2001). An experimental investigation of the frictional pressure drop of steam–water two- phase flow in helical coils. *International Journal of Heat and Mass Transfer* 44,2601–2610
- Katto, Y. (1978). A Generalized Correlation of Critical Heat Flux for the Forced Convection Boiling in Vertical Uniformly Heated Round Tubes. *Int. J. Heat Mass Transfer* 21:1527–1542
- Katto, Y. (1979). An Analysis of the Effect of Inlet Subcooling on Critical Heat Flux of Forced Convection Boiling in Vertical Uniformly Heated Tubes. *Int. J. Heat Mass Transfer* 22:1567–1575
- Katto, Y. (1980) General Features of CHF of Forced Convection Boiling in Uniformly Heated Vertical Tubes with Zero Inlet Subcooling. *Int. J. Heat Mass Transfer* 23: 493–504
- Kind, M. (2019). Strömungsformen in Verdampferrohren, *VDI Wärmeatlas*, Heidelberg, 898–899
- Knipping, T. (2018). Kühlen kleiner Kavitäten mit verdampfenden Fluiden. *DKV-Forschungsbericht*, No. 88,
- Knipping, T., Arnemann, M., Hesse, U. u. Humpfer, F. (2014). Experimental analysis of twisted shaped spot evaporators at high heat fluxes. *Proceedings of the International refrigeration and air conditioning conference*, Purdue, paper No. 2587,
- Knipping, T., Humpfer, F., Arnemann, M. u. Hesse, U. (2015): Untersuchungen zu Drall-Spot-Verdampfern bei hohen Wärmestromdichten. *Kälte Luft Klimatechnik. (1–2)*: 28–31
- Konakov, P.K. (1946): A new correlation for the friction coefficient in smooth tubes. *Berichte der Akademie der Wissenschaften der UdSSR*. Band LI, 51, 503–506
- Lindeman, B. A., Anderson, J. M. and Shedd, T. A. (2013). „Predictive model for heat transfer performance of oblique and normally, *International Journal of Heat and Mass Transfer*, Vol. 62, 612–619
- Lopina, R. F. and Bergles, A. E. (1969). Heat transfer and pressure drop in tape generated swirl flow, *ASME. J. Heat Transfer*. 434–441
- Poiseuille, J. L. M. (1846). Recherches experimentales sur le mouvement des liquides dans les tubes de tres-petits diametres, *Academie Royale des Sciences de l'Institut de France*, IX
- Roul, M., Dash, S., (2011). Two-phase pressure drop caused by sudden flow area contraction/expansion in small circular pipes. *International Journal for Numerical Methods in Fluids*. 66. 1420–1446.
- Wellenhofer, A. (2019). Druckabfall von Gas-Flüssigkeitsströmungen in Röhren, Leitungselementen und Armaturen., *VDI Wärmeatlas*, Heidelberg
- Yagov, V. V. (2005). Heat transfer and crisis in swirl flow boiling, *Experimental Thermal and Fluid Science, Volume 29*, Issue 7, 871–883